Pergamon

Int. J. Heat Mass Transfer. Vol. 38, No. 7, pp. 1161–1171, 1995

0017-9310/95 $9.50+0.00

0017-9310(94)00248-7

Numerical modeling of multiphase plasma/soil flow and heat transfer in an electric arc furnace

SEUNGHO PAIK and HOA D. NGUYEN

Thermal Systems Code Development & Analysis, Idaho National Engineering Laboratory, EG&G Idaho, Inc., Idaho Falls, ID 83415-3880, U.S.A.

(*Received* 25 *February* 1994 *and in final form* 27 *July* 1994)

Abstract—A study on an arc melter used for waste minimization process is presented. The plasma phase of the arc and the liquid–solid phases of the molten soil are simulated simultaneously. Newtonian fluid model is used for both the plasma and the molten phases. Parametric study is made on different arc lengths and arc currents with varying input powers. Calculations show that both convective heat transfer and Joule heating mechanism yield high heat dissipation in the melt pool. It is found that the buoyancy and the surface shear driven convection established in the melt pool are the major contribution to the more uniform mixing of the molten soil. For the long arc, the gas environment above the molten soil has large heated volume while the melted soil volume is small compared to those of short arc. The induced circulation in the melt pool is stronger for the short arc than that of long arc. For the same input power, increasing current results more heat dissipation inside the melt pool than increasing voltage drop.

1. INTRODUCTION

The increased use of plasma arc in metallurgical processes and waste minimization has prompted researchers to optimize the process. Understanding of those processes requires detailed informations on both the plasma arc and the molten pool. Researches on the plasma arc have been performed by various researchers [1–4]. Because of the complex nature of the plasma, experimental work is rather limited on measuring temperature and global heat transfer rate rather than obtaining localized informations which may be important for determining the optimum operating conditions in the plasma reactor. Instead, numerical modelings of the processing have been successfully used for obtaining detailed informations. Earlier work on this subject was concentrated on modeling the near electrode regions (both anode and cathode) where the major focus of the models was studying the sheath layers formed near the electrodes [1]. The nonequilibrium effects near the electrodes were studied numerically. Good agreement between spectrometric measurements and the numerical predictions was found. Tsai and Kou [2] studied the cathode-geometry effect on the flow and temperature fields of the welding arcs. They found that the calculated flow and temperature fields were sensitive to the current density distribution along the cathode tip. Pfender [3] discussed the various heat transfer modes in the plasma arc. Recent work of Gonzalez *et al.* [4] focused on studying the metal vapor effects on the heat transfer mechanism during the metal scraping using transferred arc. For the moderate current intensities, they concluded that the presence of the metal vapor significantly affects the radiation heat transfer. Heat conduction in the anode region was considered in their work. The use of arc plasma for refractory metal oxides has been considered by Taniuchi [5]. For this application, the plasma interaction with the processing material was the most important factor to design the optimized processing reactor.

For the melt pool, there are many researches found in the literature mostly related to metal welding. Much numerical work is focused on the metal pool flow and heat transfer. A comprehensive review on this subject was performed by Szekely [6], and interested readers are referred to ref. [6]. For the melt pool composed of soil, Hawkes [7] considered the natural convection effect on the soil–melt shape during the *in situ* vitrification process. By considering the Joule heating inside the melt, the temperature and flow fields were obtained inside the melt.

So far, most of the previous studies on this subject either consider the arc plasma region only or molten material domain only. However, informations on the interaction between the plasma arc and molten material are crucial to understand the process. Gu *et al.* [8] studied the plasma arc and molten metal pool interaction with vapor contaminant effect. The metal pool is treated as an anodic liquid pool in their work. Inclusion of the liquid pool convection was considered without the phase change of the soil in their work. In the present paper, study is focused on the plasma arc reactor for the waste minimization process. The interaction of the plasma and the molten pool (usually composed of contaminated soils) is studied by considering the flow, temperature, and electromagnetic

NOMENCLATURE

B	magnetic field
C_p	specific heat at constant pressure
dV	differential volume
E	electric field
h	specific enthalpy
I	total current
j	current vector
k	Boltzmann constant
L_m	latent heat of soil
n	number density
p	pressure
r	radial coordinate
r	position vector
r_0	radius of cathode spot
T	temperature
T_0	reference temperature [= 273 K]
T_{melt}	soil melt temperature [= 1473 K]
u	axial velocity
u	velocity vector
v	radial velocity
V	voltage
V_{drop}	voltage drop
x	axial coordinate.

Greek symbols

γ	surface tension
κ	thermal conductivity
μ	viscosity
μ_0	magnetic permeability at vacuum [= 1.26×10^{-6} H m^{-1}]
ρ	global density
σ	electrical conductivity
ϕ	electric potential.

Subscripts

i	ions
m	soil melt
P	plasma
r	radial coordinate
x	axial coordinate.

fields inside the reactor. The molten liquid and solid soil interface is treated by using the algorithm described by Basu and Date [9].

In the following, the mathematical model with assumptions used is presented. The numerical validation studies are performed for both the plasma and the molten pool regions by comparing results with previously published ones. Finally, results and discussions on the present work are presented.

2. MATHEMATICAL MODEL

The geometry considered in this study is shown in Fig. 1. The calculation domain is divided into the plasma gas and the soil (either liquid or solid) regions. The dimension of the soil volume is fixed while the plasma arc length (gap; the distance between the cathode tip and the soil surface) is varied for the calculations. The dimension of the reactor used in this study resembles the experimental set-up by Kong *et al.* [10] which has been set up for the thermal waste treatment.

2.1. *Assumptions*

In this study, the following assumptions are made:

1. A steady, 2D axisymmetric, and laminar plasma and molten pool flow prevails. The transient behavior of the reactor is not an objective of this study. Even though there are many factors which may disturb the axisymmetric nature of the problem, we believe the 2D calculation may yield proper informations for present purposes. The laminar flow assumption is reasonable for the high viscosity region of the plasma and the molten pool.

2. Local thermodynamic equilibrium (LTE) is assumed in order to simplify mathematical formulations. The effect of nonequilibrium addressed by Hsu and Pfender [1] is not considered in this study. As a consequence, the plasma is treated as a single continuous fluid with only one representative temperature for the flow. Likewise, the molten material is treated as a homogeneous liquid whose thermophysical properties are functions of the temperature only.

3. No interface deformation is considered. Interface between the plasma arc and the molten pool is fixed as a flat surface. This is the most serious restriction considering the fact that the strongly plasma jet impinges on the molten pool surface as well as boiling of the melt at the location of arc root attachment. However, this assumption is made for simplicity of the model.

4. Material volatilization effects at the plasma–molten pool interface are not included. The cathode material contaminated effects on the plasma properties are not considered. Owing to the high temperature encountered at the interface, it is expected that there is a mass transfer from the molten pool to the gas environment. However, the mass transfer at the interface is highly dependent on the material properties of the soil. Thus in this study, parametric study for basic soil composition at Idaho National Engineering Laboratory without mass transfer is considered.

5. The plasma is optically thin, which implies that re-absorption of radiation by the plasma compared with the total radiative loss over all wavelengths is insignificant. The radiations from the molten pool surface are also neglected.

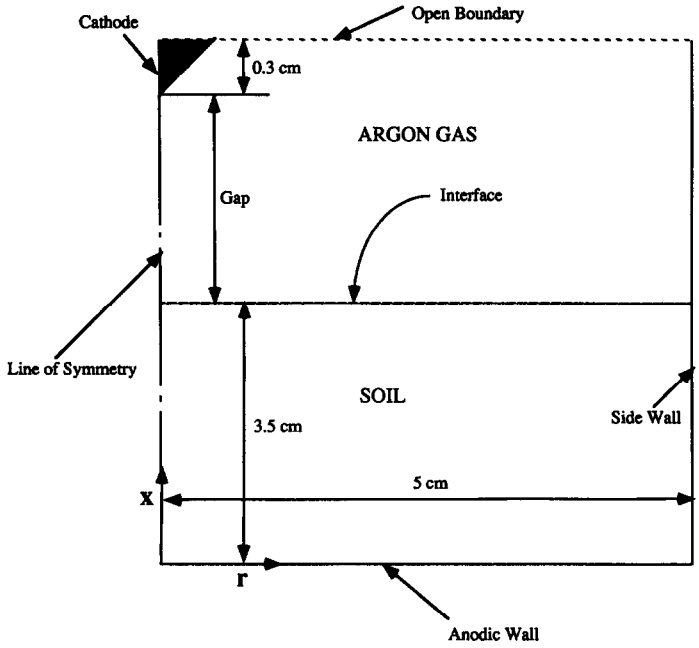

Fig. 1. Geometry of the plasma arc melter considered in this study.

6. Viscous dissipation is neglected in both the plasma arc and the molten pool regions.

2.2. *Governing equations and thermophysical properties*

Based on the above assumptions, governing equations are written in vector notations. The global mass conservation equation without considering the effect of the electrodes erosion and the material volatilization at the melt pool surface becomes

$$\nabla\cdot(\rho\mathbf{u}) = 0 \tag{1}$$

where ρ and $\mathbf{u}$ represent global density and velocity vector, respectively. The currents, $\mathbf{j}$, generated by the cathode emission are conserved as $\nabla\cdot\mathbf{j} = 0$. By use of electric potential, ϕ, defined as $\mathbf{j} = \sigma\nabla\phi$, the currents conservation equation can be written as

$$\nabla\cdot(\sigma\nabla\phi) = 0 \tag{2}$$

where σ is the electrical conductivity. Besides the gravity field, the only body force exerting on the arc is a net magnetic force, Lorentz force, generated in the arc column by an asymmetric interaction between the arc current and self-induced magnetic field. The conservation equations of momentum with the Lorentz force acting as a body force can be expressed as

$$\nabla\cdot(\rho\mathbf{uu}) = -\nabla p+\nabla\cdot(\mu\nabla\mathbf{u})+\mathbf{j}\times\mathbf{B}+\rho\mathbf{g} \tag{3}$$

where p, ρ and $\mathbf{B}$ are the pressure, gravitational force, and the self-generated magnetic field because of the current flow, respectively. Total specific enthalpy for the plasma (h_P) is defined as

$$h_P = (\tfrac{5}{2}nkT+n_iE_i)/\rho_P \tag{4}$$

where n, k, n_i, E_i, are total number density, the Boltzman constant, ion species number density and ionization energy, respectively. By using the enthalpy formulation, the governing energy conservation equation becomes

$$\nabla\cdot(\rho_P\mathbf{u}h_P) = \nabla\cdot\left(\frac{\kappa_P}{C_{pP}}\nabla h_P\right)+\frac{\mathbf{j}\cdot\mathbf{j}}{\sigma_P} +\frac{5}{2}\frac{k}{eC_{pP}}(\mathbf{j}\cdot\nabla h_P)-S_r \tag{5}$$

where κ_P, C_{pP}, S_r and e represent the plasma thermal conductivity, the specific heat at constant pressure, the optically thin radiation energy loss, and the elementary charge, respectively. The subscript P represents the plasma quantity. Equation (5) contains the convection, the conduction, the Joule heating, the transport of electron enthalpy because of the drift of the electrons, and the radiation loss terms in respective order.

The molten pool domain requires the same set of governing equations as the plasma domain. The electrically conducting molten pool is subjected to the gravity and the electromagnetic fields so that the same mass, electron charge, and momentum conservation equations should be satisfied with the molten material properties. For the energy conservation, the radiant energy and the electron drift energy contribution to the molten pool is ignored. The specific enthalpy of the soil (h_m) can be defined as

$$\begin{aligned} h_m &= C_{pm}(T-T_0) \quad \text{for } T < T_{melt}\\ h_m &= C_{pm}(T_{melt}-T_0)+L_m \quad \text{for } T = T_{melt}\\ h_m &= C_{pm}(T-T_0)+L_m \quad \text{for } T \geqslant T_{melt} \end{aligned} \tag{6}$$

where T_{melt} and L_m is the melt temperature and the

latent heat of melting for the soil, respectively. By using the specific enthalpy of equation (6), the energy conservation equation for the molten pool domain can be written as

$$\nabla\cdot(\rho_m \mathbf{u} h_m) = \nabla\cdot\left(\frac{\kappa_m}{C_{pm}}\nabla h_m\right) + \frac{\mathbf{j}\cdot\mathbf{j}}{\sigma_m} \tag{7}$$

where because of the electrically conducting property of the molten soil, the Joule heating term is kept with convection and conduction terms. It should be noted here that the transport of electron enthalpy due to electron drift is neglected compared to the high enthalpy of the soil.

Equations (1)–(3), (5) and (7) are the physical governing equations used in this study for the plasma and the soil region. The governing equations can be solved with any established elliptic partial differential equation solvers. In order to solve the governing equations, supplementary informations of the currents and the magnetic fields are needed. The current density may be calculated by using the Ohm's law which can be written as

$$\mathbf{j} = \sigma(\mathbf{E} + \mathbf{u}\times\mathbf{B}) \tag{8}$$

where **E**, **u** and **B** are the electric field, the magnetic field and the drift velocity of the charged particles, respectively. In the absence of externally applied magnetic field, the $\mathbf{u}\times\mathbf{B}$ term, the induced current density by the motion of the charged particles across the magnetic field is comparably small. Thus only the electric field contribution to the current is considered in this study. The self-induced magnetic field can be expressed by using the Biot–Savart law [11] expressed as

$$\mathbf{B} = \frac{\mu_0}{4\pi}\oint\frac{\mathbf{j}\times\mathbf{r}}{r^3}\,dV \tag{9}$$

where μ_0 ($= 1.26\times10^{-6}$ H m^{-1}) is the magnetic permeability of vacuum, and dV is the differential volume. In case of the free burning arc, the magnetic field is dominated by the strong axial current. Thus the inclusion of the radial current contribution does not change the obtained temperature solution fields significantly [12].

The thermodynamic and transport properties of argon at one atmospheric pressure used in this study are taken from ref. [12]. The data of the radiational energy loss are taken from the experimental work of Evans and Tankin [13]. All the plasma property data are provided in a tabulated form with every 1000 K temperature intervals from 1000 to 25000 K. The properties between the specified temperature intervals are linearly interpolated. The density and the viscosity of the soil are taken from Buelt *et al.* [14] which is shown in Fig. 2. The other thermophysical properties of the soil used for this study are from Henderson and Taylor [15] and shown in Table 1. Due to the lack of data points for the thermophysical properties of soil, linear interpolation is used in the calculation for the properties between the data points.

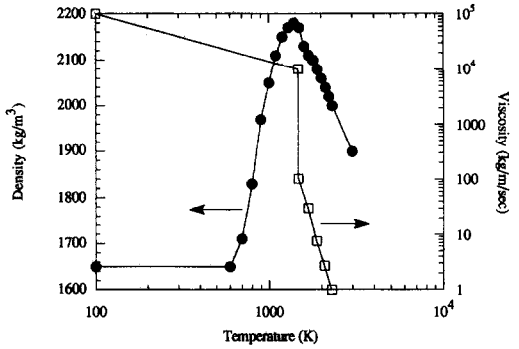

Fig. 2. Temperature dependence of the soil's density and viscosity at Idaho National Engineering Laboratory. The properties are taken from Buelt *et al.* [14].

2.3. *Boundary conditions*

At the wall, constant temperature boundary condition and no slip boundary condition for the velocity fields are used in this study. High electrical conductivity with floating current condition for the electric field are imposed at the bottom anodic wall surface. For the centerline ($r = 0$), symmetry boundary condition with zero normal velocity component is specified. Since no interface deformation between the molten pool and plasma phase is considered in this study, normal velocity at the interface is set to zero with shear stress continuity requirement across the interface. It should be mentioned that the usual boundary condition for the tangential velocity at the interface in welding problem considers the surface tension driving force (Marangoni force) only. However the surface tension is a complicated function of material composition and the information about the thermal behavior of the surface tension for the present problem is not available. Moreover, for the free burning arc problem the induced convective flow is much stronger and tends to overcome the surface tension induced force [8]. Thus, the Marangoni effect is not considered in this study. The heat flux continuity at the interface is used for the energy conservation. No shielding gas is used in this study. The above mentioned boundary conditions can be translated into mathematical expressions as follows:

At the wall:

$$u_p = v_p = u_m = v_m = 0$$

Table 1. Soil thermophysical properties

Temperature [K]	C_{pm} [J/kg^{-1} K^{-1}]	κ_m [W m^{-1} K^{-1}]	σ_m [Ω^{-1} m^{-1}]
0.0	881	0.2	0.001
673	1096	0.23	0.001
1073	1166	0.45	0.016
1428	1284	8.5	0.98
1773	1284	18	5.6
2173	1284	50	20
2573	1284	80	44
5000	1284	80	88

$$T = 1000\,\mathrm{K}$$

$$\left.\frac{\partial \phi}{\partial r}\right|_{r=R} = 0, \left.\frac{\partial^2 \phi}{\partial x^2}\right|_{x=0} = 0. \tag{10}$$

At the interface ($x = 3.55$ cm):

$$u_p = u_m = 0,$$

$$-\mu_p\left[\frac{\partial v_p}{\partial x} + \frac{\partial u_p}{\partial r}\right] = -\mu_m\left[\frac{\partial v_m}{\partial x} + \frac{\partial u_m}{\partial r}\right]$$

$$-\kappa_p \frac{\partial T_p}{\partial x} = -\kappa_m \frac{\partial T_m}{\partial x}$$

$$-\sigma_p \frac{\partial \phi_p}{\partial x} = -\sigma_m \frac{\partial \phi_m}{\partial x}. \tag{11}$$

τ and q are the stress tensor and the heat flux which are defined in ref. [16].

At the center:

$$\frac{\partial u_p}{\partial r} = \frac{\partial u_m}{\partial r} = \frac{\partial T_p}{\partial r} = \frac{\partial T_m}{\partial r} = \frac{\partial \phi}{\partial r} = v_p = v_m = 0. \tag{12}$$

At the top of the reactor (open boundary):

$$\frac{\partial u_p}{\partial x} = \frac{\partial u_m}{\partial x} = \frac{\partial T_p}{\partial x} = \frac{\partial T_m}{\partial x} = v_p = v_m = 0, \phi = V_{drop} \tag{13}$$

where V_{drop} is the voltage specified by the input power. At the cathode tip, the current boundary condition is imposed, which represent cathode emission of electrons. The current is specified at 1 mm below the cathode with an exponential function as

$$j_x|_{x=3\,\mathrm{mm}} = j_{x_{max}} \exp(-r/r_0) \tag{14}$$

where $j_{x_{max}}$ is the maximum current at the cathode tip and r_0 is the cathode spot radius. Both $j_{x_{max}}$ and r_0 vary with the operating condition and the cathode shape and can be determined from experimental observation [12].

3. NUMERICAL METHOD AND VALIDATION TEST

The momentum and the mass conservation equations are solved by using SIMPLEC algorithm [17]. The energy and the electron conservation equations are solved by using the same procedure described by Patankar [18]. For the solid–liquid boundary, the approach used by Basu and Date [9] is adopted in this study. Details of the solid–liquid boundary treatment is referred to Basu and Date. In the solid domain, the viscosity is set to 10^{16} kg m^{-1} s^{-1} in order to ensure no flow is allowed.

In order to validate our physical model and computer code, comparison is made on the temperature profile for the argon plasma arc region. Similar comparison is made by Hsu [12] in order to verify their model on the free burning arc. Figure 3 shows isotherm in the plasma domain. The same boundary conditions and the operating conditions as those of Hsu are used in order to compare with the experimental data. The results are slightly different from Hsu's results near the anode region which can be explained by the different grid resolution (32×22) for the present calculation. By increasing the axial direction resolution, we obtained stiff temperature gradient near the anode surface. Reasonable agreement with the experimental data is found for the isotherms of the plasma arc.

Another comparison is made for the molten pool region calculation. For this validation test, we selected the validation test performed by Basu and Date [9]. In their calculation, the surface is assumed to be driven by the surface tension gradient which results in replacing the boundary condition, i.e. equation (11b) with the Marangoni force which can be written as

$$\mu_m \frac{\partial v}{\partial x} = -\frac{\partial \gamma}{\partial T}\frac{\partial T}{\partial r} \tag{15}$$

where γ is the surface tension. The melt depth and width resulting from laser welding for Al–4.5% Cu is compared. The beam diameter is 1.0 mm and the predicted depth and width is compared with the experimental results obtained by Sekhar [19]. The physical properties used for this comparison can be found in refs. [9, 19]. The Lorentz force term as well as the Ohmic heating term in momentum and energy conservation equations were not used for the simulation. Table 2 shows the compared results. In general, good agreements are found with the numerical results by Basu and Date.

4. RESULTS AND DISCUSSIONS

There are many issues that need to be addressed on designing the arc melter for waste minimization [20]. One of primary purposes of the present study is to find out the effect of the distance between the cathode and the melt pool surface. Arc length is an important factor on determining steady state operating condition for an arc reactor [10] which can practically be operated from as close as the cathode submerged into the melt pool to as far from the interface as the arc can be sustained. When the cathode is submerged into the melt pool, the heating is primarily via the Joule heating between the electrodes. Another consideration is given to the arc current variation. Two different arc current cases, i.e. 200 A and 300 A, are considered with different arc powers (ranges from 5 to 15 kW) in this study. The same cathode tip radius of 200 A [1, 12] is used for the 300 A case for the calculation.

Figure 4 shows isotherms in the arc reactor for the arc current $I = 200$ A and 5 kW input power with different arc lengths. The melt front in the soil region shows a bowl shape with maximum temperature occurring at the bottom of the reactor because of the high current density collected at the bottom. In Fig. 4, the maximum temperature near the bottom of the

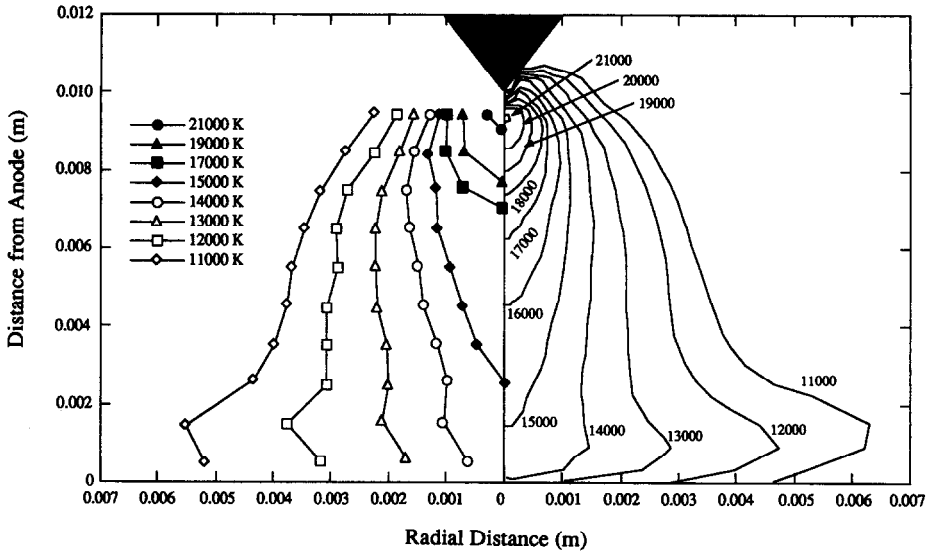

Fig. 3. Comparison of the free burning arc (200 A) isotherms with the experimental measurement performed by Hsu and Pfender [1]. Isotherms on the left-hand side is the experimental results and those on the right-hand side is the present calculation.

Table 2. Comparison of the melt widths and depths with previous results

$q \times 10^8$ [W m^{-2}]	Width [mm] Sekhar (exp.) [19]	Basu and Date [9]	Present results	Depth [mm] Sekhar (exp.) [19]	Basu and Date [9]	Present results
2.43	0.238	0.294	0.287	0.146	0.049	0.053
3.12	0.410	0.443	0.441	0.175	0.130	0.135
3.97	0.470	0.494	0.495	0.201	0.198	0.198
4.10	0.500	0.520	0.524	0.230	0.239	0.236
5.00	0.577	0.579	0.581	0.264	0.398	0.351
5.60	0.600	0.610	0.621	0.500	0.453	0.427

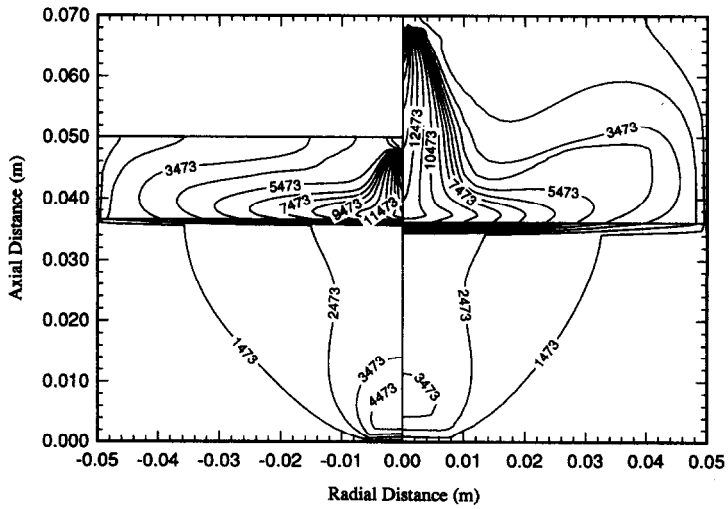

Fig. 4. Isotherms inside the plasma arc melter (from 1473 to 19 473 K with 1000 K increment) for a current density of 200 A and 5 kW input power. Results on the left-hand side are for the 1 cm arc length case (gap = 1 cm) and those on the right-hand side are for 3 cm arc length case (gap = 3 cm).

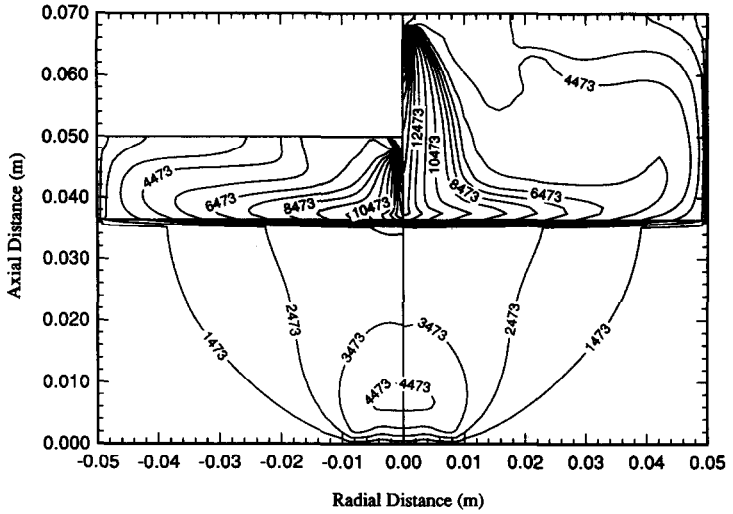

Fig. 5. Isotherms inside the plasma arc melter (from 1473 to 19 473 K with 1000 K increment) for a current density of 300 A and 7.5 kW input power. Results on the left-hand side are for the 1 cm arc length case (gap = 1 cm) and those on the right-hand side are for 3 cm arc length case (gap = 3 cm).

reactor increases as the arc length becomes shorter. However, for the higher input power (i.e. 7.5 kW in Fig. 5) the maximum temperature near the bottom of the reactor remains same for different arc length cases, instead the surface temperature near the melt core increases for short arc case. In Fig. 6, high current density is found near the core region of the soil because of the relatively high electrical conductivity of the soil at the high temperatures. The high current density induces the high Joule heat dissipation which results in the higher temperatures in that region. Figure 7 shows that the induced flow fields in the molten soil region have strong clockwise convection occurring on the right-hand side of the reactor. There are two factors for this convection. One is because of the shear stress induced flow at the interface. The arc jet after impinging on the interface makes a sharp radially outward turn which induces high radially outflow at the interface. The other is owing to the buoyancy force induced by the high temperature at the bottom of the reactor. Because of the large density difference caused by the temperature gradient inside the molten soil, the induced natural convection force contributes the clockwise convection in the melt pool. It should be mentioned here that for the cases we consider, the effect of the electromagnetic force in the melt pool is not causing major changes for the flow directions as found by *Gu et al.* [8] for the metal pool case because

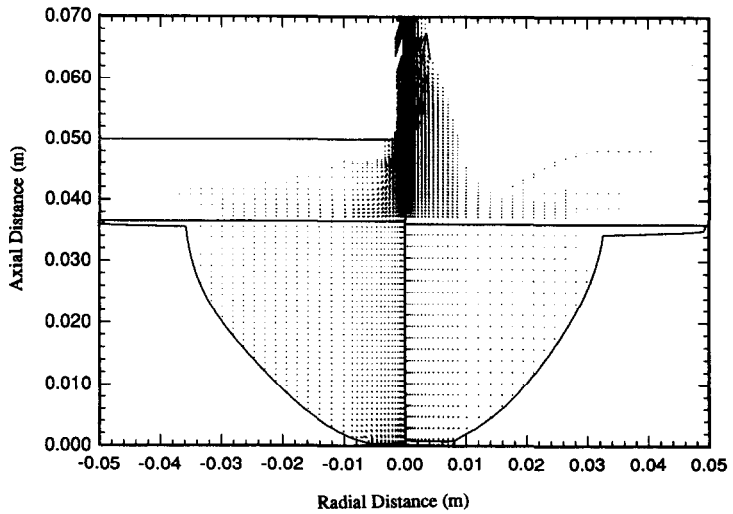

Fig. 6. Current vector inside the plasma arc melter for a current density of 200 A and 5 kW input power. The solid line represents the melting boundary inside the soil. Results on the left-hand side are for the 1 cm arc length case (gap = 1 cm) and those on the right-hand side are for 3 cm arc length case (gap = 3 cm).

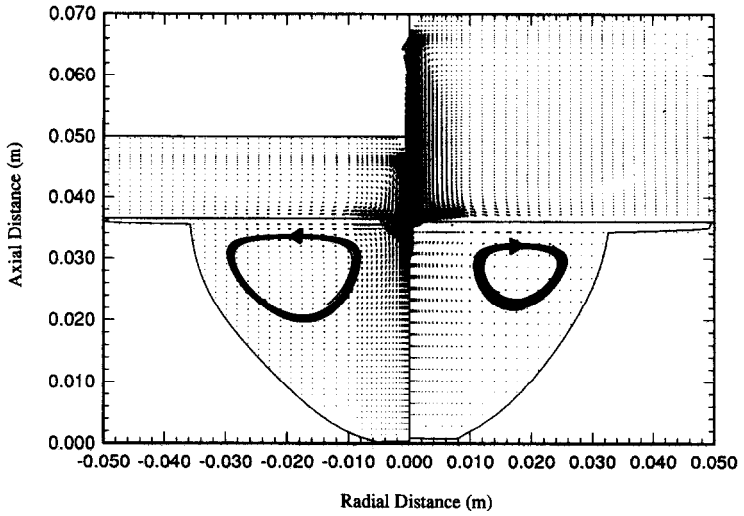

Fig. 7. Velocity vector inside the plasma arc melter for a current density of 200 A and 5 kW input power. The solid line represents the melting boundary inside the soil. The loops inside the melt represent streaklines. Results on the left-hand side are for the 1 cm arc length case (gap = 1 cm) and those on the right-hand side are for 3 cm arc length case (gap = 3 cm).

of the low electrical conductivity of the soil. The ratio of the electromagnetic force to the buoyancy force is defined [21] as

$$\text{Ratio} = \frac{\mu_0 I^2 C L_R^2 \alpha_j^4}{\rho \pi^2 L g \beta \Delta T} \tag{16}$$

where I is the total current, α_j is the current distribution over the melt surface, L_R is the melt pool radius, and C is the constant depending on the arc operating mode (in this study, the cathode spot mode is considered. Thus $C = 8$ is used). Values of the ratios in equation (16) based on the parameters considered in this study are order of 0.1. Thus, the contribution of the Lorentz force on the melt pool convection is not significant compared to that of buoyancy force. Besides, the strong tangential shear at the interface intensifies the clockwise convection in the melt pool. It has been noticed by Oreper and Szekely [21] that the clockwise circulation (i.e. radially outward convection at the melt surface) may yield shallow melt pool in traditional welding. However, in their study the Joule heating through the melt is not considered. The Joule heating effect on the melt pool shape was shown experimentally by Kou and Sun [22]. The current arriving at the melt surface is penetrating vertically through the melt and generates a deeper melt pool than that without the current. These combining effects of the convection and the Joule heating heat transfer yields an efficient way of melting the soil in the arc melter.

The effect of the arc length is shown in Figs. 4–7. For the arc length of 3 cm and total current 200 A case (Fig. 4), the melted volume of the soil is about 10% less than the arc length of 1 cm case. However, for the long arc, larger volume of the environment gas is heated up to 2000 K which may give favorable condition for the off-gas emitting from the melt surface during contaminated waste treatment. Treatment of the off-gas specially high volatile pressure materials from the melt is one of the major concerns of waste minimization process [20]. For the efficient treatment of the volatile gases, longer residence time of the off-gas in hot stream is desirable. During the process, this effect should be considered to determine the arc length. Similar effects on the temperature of the environment gas are found for the increased arc current. For the high current case, the gas temperature is higher than that of low arc current. Thus, both effects of the melt pool volume and the heated gas volume should be considered during the process.

Figures 8–10 show the interfacial temperature, current, and velocities for different operating conditions. For the short arc, the temperature at the interface is higher than for the long arc as one expected. Likewise, the maximum currents at the interface for the short arc are higher than those of the long arc. For the long arc, slightly higher currents than those of short arc can be found far from the arc core since the electrical conductivities of the plasma and the melt pool are relatively evenly distributed over the interface. This effect becomes noticeable for the high input power case. For higher input power case (7.5 kW), the currents and the temperatures at the interface far from the arc core show slight increase for the longer arc case. This is because that for the high input power with long arc, the increased gas temperature spread more uniformly above the molten pool and increase the molten pool surface temperature and electrical conductivity. The tangential velocity (i.e. radial direction velocity) at the interface shows that the maximum velocity can be as high as 20 m s^{-1}. The maximum velocity increases as the current increases since the electromagnetically induced plasma flow increases as the current increases. The velocity increases as the

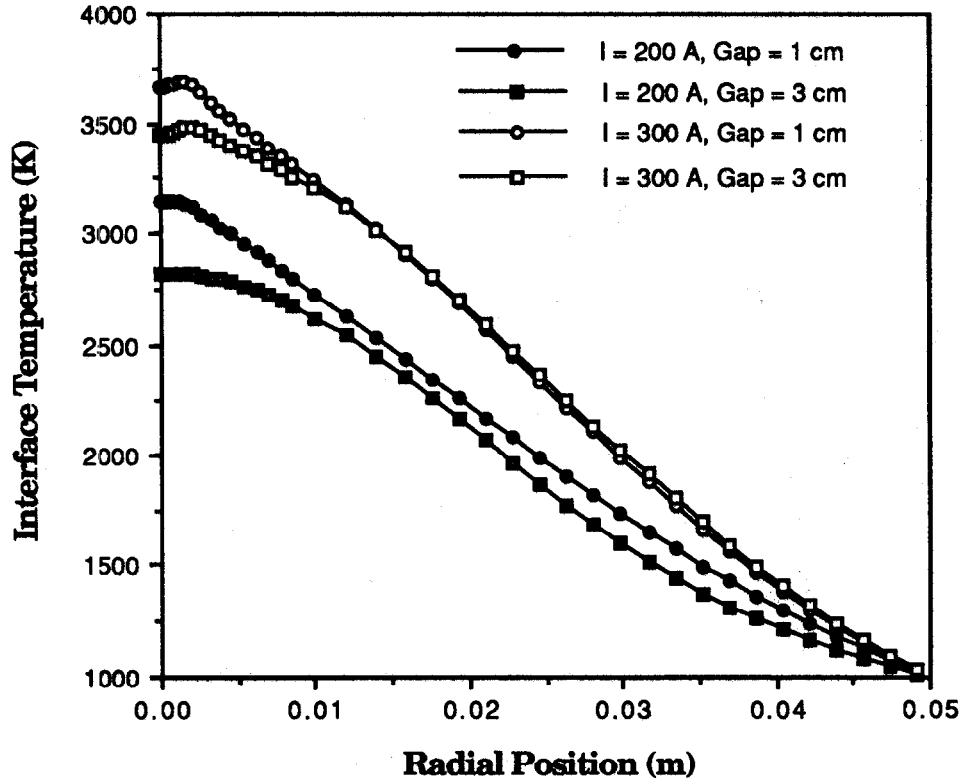

Fig. 8. Plasma–soil interfacial temperature profile.

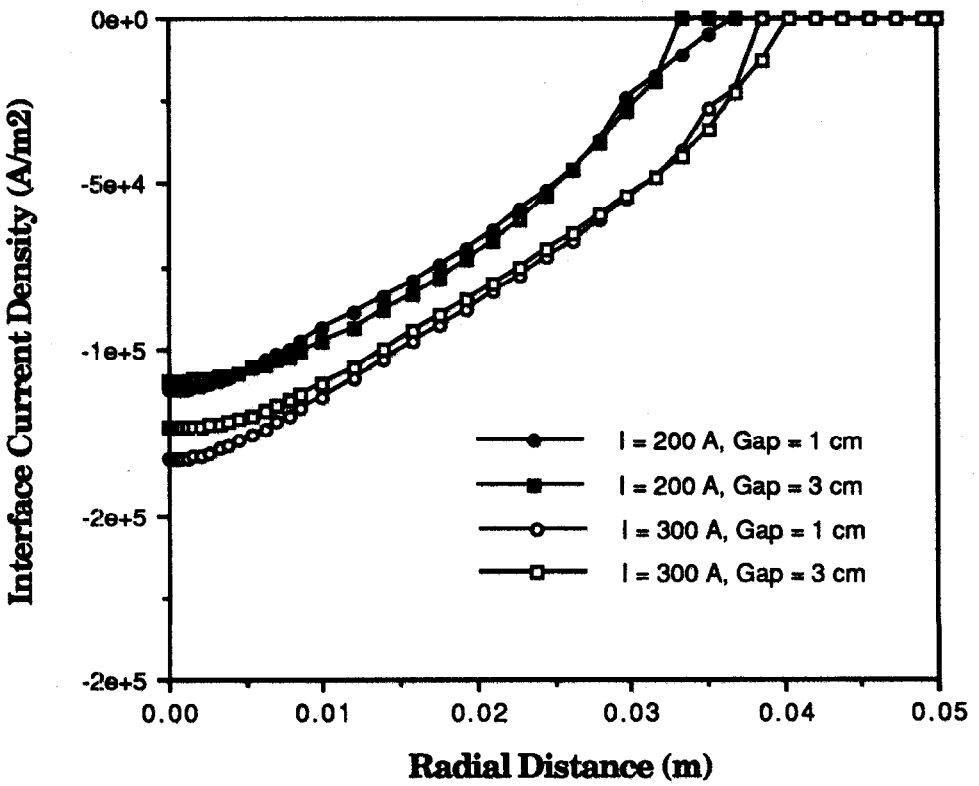

Fig. 9. Plasma–soil interfacial normal current profile.

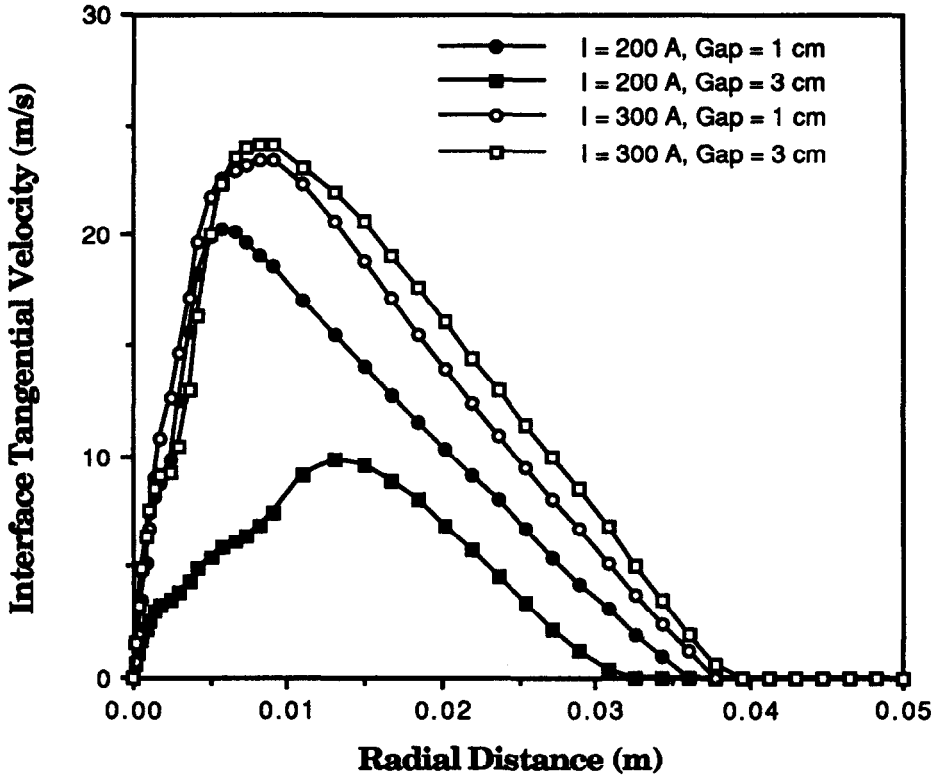

Fig. 10. Plasma–soil interfacial tangential velocity profile.

distance from the stagnant point increases initially and reaches maximum in magnitude and decreases because the viscosity increases as temperature decreases.

Finally, soil heating efficiency is calculated for different arc operating conditions and listed in Table 3. The efficiency is defined as the ratio between the power absorbed by the melt pool to the total power of the reactor. The melted soil volume percentage to the total soil volume is also listed in Table 3. By comparing the melted volume percentage, increasing the voltage for the same current does not affect the melt volume significantly. Rather, increasing the arc current has significant effects on having the large melted volume. This fact is mainly because the heating mechanism of the soil is the Joule heating. By increasing the arc current, heat is transferred to the soil more efficiently. However, when the material volatility is the major concern of designing, the selection of high current flow may increase volatility of the materials in the reactor. Besides, high current results in fast electrode erosion which may lead to short life time of the electrodes. The absorbed power by the soil decreases as increasing the arc length for the same power. This is in qualitative agreement with the results by Qian *et al.* [23].

5. CONCLUSIONS

(1) A computer model for simulating steady-state, 2D axisymmetric heat, fluid flow, and electromagnetic fields is developed for the calculation of the arc plasma and molten pool regions for the waste minimization process. The interaction between the plasma and the pool regions are treated in a consistent manner by using interface physical quantity continuity assumption.

(2) The convective heat transfer and the joule heat-

Table 3. Percentage of the power absorbed by the melt pool to the total power for different operating conditions

Total power [kW]	Gap = 1 cm		Gap = 3 cm	
	I = 200 A	I = 300 A	I = 200 A	I = 300 A
5	38.3(28.50)†	46.7(37.53)	35.2(27.68)	42.8(38.28)
7.5	27.5(28.82)	37.4(37.75)	26.0(27.69)	35.9(41.43)
10	20.9(28.95)	33.9(38.05)	19.4(28.68)	29.7(43.47)
15	16.9(29.21)	27.1(38.43)	15.3(29.18)	22.3(46.32)

† The number in the parenthesis is the percent ratio of the melt volume to the total soil volume.

ing mechanisms are responsible for heating the molten soil for the waste minimization process.

(3) For the different length of the arc at the same total power and currents, the currents arriving at the melt pool surface make little difference for the heating of the melt pool. Instead, the convective heat transfer from the surface causes the different melt shape in the pool.

(4) For the same currents, the longer arc heats up larger volume of the gas environment while the melt pool volume is smaller than that of short arc. In case off-gas treatment is considered, the effect of large volume of high temperature zone may give favorable environment.

(5) Inside the melt pool, short arc induces strong convection which may lead to uniform mixing of materials inside the pool. If the localized gas heating effect is not desirable, the short arc mode operation is recommended for the thermal waste treatment.

(6) Increasing power via increasing voltage drop dissipates more heat to the environment gas than to the soil. If large volume of melted soil is desired, increasing the power by increasing current is a more efficient way of heating the soil. However, the fact that the high currents induce fast electrode erosion should be considered for finding the optimum operating conditions.

Acknowledgements—The authors thank Mr E. B. Nielson for Figs. 2 and 3. Valuable comments from Dr P. C. Kong are gratefully acknowledged. The work was performed under the auspices of the U.S. Department of Energy, contract DE-AC07-76-ID01570, and was supported in part by the Buried Waste Integrated Demonstration Program.

REFERENCES

1. K. C. Hsu and E. Pfender, Two-temperature modeling of the free-burning, high-intensity arcs, *J. appl. Phys.* **54,** 3818 (1983).
2. M. C. Tsai and S. Kou, Heat transfer and fluid flow in welding arcs produced by sharpened and flat electrodes, *Int. J. Heat Mass Transfer* **33,** 2089 (1990).
3. E. Pfender, Energy transport in thermal plasma, *Pure Appl. Chem.* **52,** 1773 (1980).
4. J. J. Gonzalez, A. Gleizes, P. Proulx and M. Boulos, Mathematical modeling of a free-burning arc in the presence of metal vapor, *J. appl. Phys.* **74,** 3065 (1993).
5. K. Taniuchi, Arc-plasma reduction of some refractory metal oxides, *High Temp. Mater. Processes* **11,** 369 (1993).
6. J. Szekely, *Fluid Flow Phenomena in Metal Processing.* Academic Press, New York (1979).
7. G. L. Hawkes, Influence of natural convection on melt shape during in situ vitrification, *ASME Heat Transfer Geophys. Media,* HTD **172,** 1 (1991).
8. L. Gu, R. Jensen, A. E. Arntsberg and J. A. Bakken, Study on silicon vapor contaminated argon arcs and the metal pools, *Proceedings of the 11th International Symposium on Plasma Chemistry* **1,** 222, Loughborough, England, 22–27 August (1993).
9. B. Basu and A. W. Date, Numerical study of steady state and transient laser melting problems—I. Characteristics of flow field and heat transfer, *Int. J. Heat Mass Transfer* **33,** 1149 (1990).
10. P. C. Kong, J. D. Grandy, A. D. Watkins, T. L. Eddy and G. L. Anderson, Bench-scale arc melter for R&D in thermal treatment of mixed wastes, EGG-MS-10646, Idaho National Engineering Laboratory (INEL), Idaho Falls, ID (1993).
11. J. D. Jackson, *Classical Electrodynamics.* Wiley, New York (1975).
12. K. C. Hsu, A self-consistent model for the high intensity free-burning argon arc, Ph.D. Thesis, University of Minnesota (1982).
13. D. L. Evans and R. S. Tankin, Measurement of emission and absorption of radiation by an argon plasma, *Phys. Fluids* **10,** 1137 (1967).
14. J. L. Buelt, V. F. FitzPatrick, C. L. Timmerman, J. G. Carter and K. H. Oma, In situ vitrification of transuranic waste: an updated systems evaluation and applications assessment, PNL-4800 suppl-1, US-70 (1987).
15. R. B. Bird, W. E. Stewart and E. N. Lightfood, *Transport Phenomena.* Wiley, New York (1960).
16. J. B. Henderson and R. E. Taylor, TPRL-1238, Thermophysical Properties Research Laboratory, School of Mechanical Engineering, Purdue University, West Lafayette, IN (1993).
17. J. P. Vandoormal and G. D. Raithby, Enhancements of the SIMPLE method for predicting incompressible fluid flows, *Numer. Heat Transfer* **7,** 147 (1984).
18. S. V. Patankar, *Numerical Heat Transfer and Fluid Flow* (1st Edn). Hemisphere, New York (1980).
19. J. A. Sekhar, Rapid solidification of alloy substrates by lasers and electron beams: heat flow modelling and solidification morphology, Ph.D. Thesis, University of Illinois at Urbana-Champaign (1982).
20. A. D. Donaldson, R. J. Carpenedo and G. L. Anderson, Melter development needs assessment for RWMC buried wastes, EGG-WTD-9911, Idaho National Engineering Laboratory (INEL), Idaho Falls, ID (1992).
21. G. M. Oreper and J. Szekely, Heat- and fluid-flow phenomena in weld pools, *J. Fluid Mech.* **147,** 53 (1984).
22. S. Kou and D. K. Sun, Fluid flow and weld penetration in stationary arc welds, *Metall. Trans.* **16A,** 203 (1985).
23. F. Qian, B. Farouk and R. Mutharasan, Modeling of fluid flow and heat transfer in the plasma region of the electric arc furnace, *Proceedings of the 29th National Heat Transfer Conference,* Atlanta, Georgia, HTD **248,** p. 53, August (1993).